Synthetic and Systems Biotechnology 10 (2025) 774–782

Contents lists available at ScienceDirect

Synthetic and Systems Biotechnology

journal homepage: www.keaipublishing.com/en/journals/synthetic-and-systems-biotechnology

Original Research Article

Development of ultrasound-visualized tumor-targeting engineered bacteria for precise tumor therapy

Li Qu, Zhou Chi, Zhen-Ping Zou, Ying Zhou, Bang-Ce Ye *

Lab of Biosystems and Microanalysis, State Key Laboratory of Bioreactor Engineering, East China University of Science and Technology, Shanghai, 200237, China

ARTICLE INFO

Keywords:
Bacterial therapy
Ultrasound visualization
Targeting tumors
Diagnosis
Treatment

ABSTRACT

In situ imaging diagnosis and precise treatment of deep tumor tissues are hotspots in life sciences and medical research. In recent years, using focused ultrasound to remotely control engineered bacteria for drug release has become one of the methods for precise *in vivo* drug delivery. However, non-visualized engineered bacteria pose challenges for precise control within the body. Therefore, there is an urgent need for an engineered bacterial vector capable of deep tissue imaging to precisely locate bacteria *in vivo*. Acoustic reporter genes (ARGs) are biological elements used for deep tissue imaging, with gene clusters over 8 kb. However, ARGs are often tested on plasmids, which hinders stable expression *in vivo* and limits the space for inserting components that regulate drug release. Therefore, we used the attenuated *Salmonella typhimurium* VNP20009, known for its tumor-targeting ability, as the chassis bacteria. By using CRISPR-Cas9 technology, we inserted ARGs into the genome and optimized the promoter strength and copy number for ARG expression, constructing ultrasound-visible engineered bacteria expressing gas vesicles on the genome. Additionally, by knocking out the stress protein gene *htrA* in VNP20009, we increased the maximum injection dose by tenfold and the tumor specificity by a hundredfold. The constructed ultrasound-visible engineered bacteria can stably synthesize gas vesicles and output ultrasound signals while directly carrying drug plasmids for tumor therapy. Our research provides an effective vector for diagnosis and precise treatment.

1. Introduction

The development of synthetic biology has made the application of engineered bacteria in tumor therapy a rapidly growing field [1–3]. The tumor microenvironment, characterized by hypoxia, nutrient richness, and immune barriers, creates ideal conditions for bacterial tumor targeting [4–8]. Engineered bacteria can be designed to express exogenous genes, enabling them to perform various functions such as therapy and imaging [9–12]. *In situ* imaging of these bacteria can assist in tumor visualization and pinpoint the location of bacteria at the lesion site, facilitating precise, remote-controlled drug release [13].

Numerous biological elements have been developed for imaging, including fluorophores for optical imaging [14,15], melanin for photoacoustic imaging [16], and gas vesicles for ultrasound imaging [17]. Among these, ultrasound imaging offers advantages such as safety, affordability, non-invasiveness, and strong penetration, making it more versatile than optical imaging [18–22]. Therefore, developing stable ultrasound-visualized engineered bacteria is crucial for achieving efficient and precise integrated *in situ* diagnosis and treatment.

To explore *in vivo* ultrasound imaging, various gas vesicles from different sources have been developed as ultrasound contrast agents [17,23,24]. Gas vesicle structures were first discovered in cyanobacteria, providing buoyancy and light refraction for cells, and similar structures were found in halophilic archaea [25]. Mature gas vesicles are spindle-shaped or cylindrical, composed of protein walls without lipids or carbohydrates, and are only 2 nm thick, formed by a layer of 7–8 kDa structural proteins [26]. Known gas vesicles involve approximately 8–14 different proteins during formation, with encoding genes present in ARGs. GvpA is the main structural protein, forming 4.6 nm ribs nearly perpendicular to the vesicle's long axis, found in nearly all ARGs. Other proteins assist in assembling GvpA to form gas vesicles, with some auxiliary proteins influencing the vesicle configuration.

In bacterial tumor therapy, *Salmonella typhimurium* VNP20009 is commonly used as an engineered bacterium. Research has shown that knocking out the *htrA* gene in VNP20009 improves the tumor-targeting ability of the engineered bacteria [27,28]. In this study, we utilized the

Peer review under the responsibility of Editorial Board of Synthetic and Systems Biotechnology.
* Corresponding author.
E-mail address: bcye@ecust.edu.cn (B.-C. Ye).

https://doi.org/10.1016/j.synbio.2025.03.009
Received 7 January 2025; Received in revised form 12 March 2025; Accepted 26 March 2025
Available online 1 April 2025

CRISPR-Cas9 system to integrate ARGs into the *htrA* locus of the VNP20009 genome, thereby disrupting the *htrA* gene [29,30]. Subsequently, we optimized the strength and quantity of the promoters regulating ARGs using RED homologous recombination [31]. Finally, we knocked catabolite activator protein (CAP) binding site [32] and plac-regulated T7 RNA polymerase (*T7RNAP*) into the VNP20009 genome, using two pT7 promoters to regulate the expression of ARGs' structural and auxiliary proteins, respectively, to construct

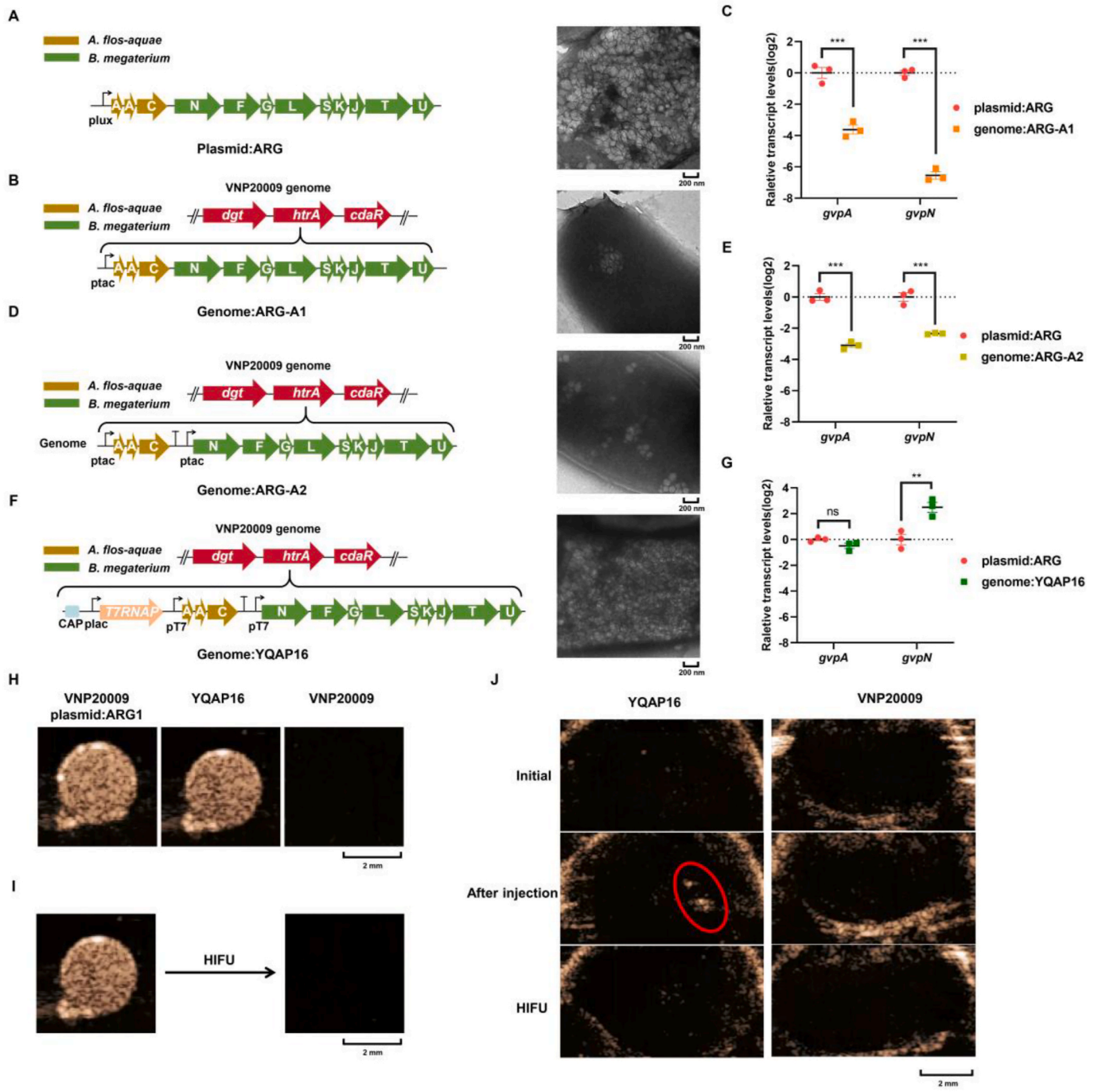

Fig. 1. Construction of ultrasound-visualized engineered bacterial strains. (A) Plasmid map and TEM imaging of VNP20009 expressing gas vesicles through plasmid expression. (B) Schematic diagram of ARGs knock-in within the VNP20009 genome, and TEM imaging of ARG-A1. (C) Comparison of transcription levels of *gvpA* and *gvpN* between VNP20009 carrying ARGs plasmid and ARG-A1. (n = 3, data presented as mean ± SEM). (D) Schematic diagram of two-segment transcription expression of ARGs in the genome, and TEM imaging of ARG-A2. (E) Comparison of transcription levels of *gvpA* and *gvpN* between VNP20009 carrying ARGs plasmid and ARG-A2. (n = 3, data presented as mean ± SEM). (F) Mediating ARGs transcription in the genome with T7RNAP, and TEM imaging of YQAP16. (G) Comparison of transcription levels of *gvpA* and *gvpN* between VNP20009 carrying ARGs plasmid and YQAP16. (n = 3, data presented as mean ± SEM). (H) Ultrasound imaging of different engineered bacteria, with a density of 1×10^9 cfu/mL. (I) Ultrasound imaging of YQAP16 before and after HIFU, with a density of 1×10^9 cfu/mL. (J) Ultrasound imaging of tumors after intratumoral injection of engineered bacteria. "Initial" represents before injection, "After injection" represents after intratumoral injection of engineered bacteria, and "HIFU" represents the ultrasound imaging after HIFU explosion of bacterial gas vesicles. The engineered bacteria concentration used is 1×10^9 cfu/mL, with an intratumoral injection of 100 μL. The circled area indicates the region of ultrasound signal change. Scale bars: 200 nm (A, B, D, F), 2 mm (H, I, J).

ultrasound-visualized engineered bacteria. These bacteria stably express gas vesicles, with quantity and shape, as well as ultrasound signals similar to plasmid-expressed gas vesicles, achieving *in situ* ultrasound imaging of engineered bacteria. Moreover, ultrasound-visualized engineered bacteria with disrupted *htrA* gene increased the maximum injection dose 10-fold, enhanced tumor targeting by 100-fold, and reduced signal interference during imaging. Transforming plasmids that express nbPD1 [33] and nbCTLA-4 [34] into ultrasound-visualized engineered bacteria confirms the compatibility of drug expression with gas vesicle expression. In mice with solid tumors, these engineered bacteria for integrated diagnosis and treatment can express nbPD1 and nbCTLA-4 to effectively inhibit tumor growth.

2. Results

2.1. Construction of ultrasound-visualized engineered bacteria expressing gas vesicles on the genome

To achieve *in situ* imaging of engineered bacteria in tumors, we first constructed a strain capable of stably emitting ultrasound signals over an extended period *in vivo*. The gene for the stress protein HtrA was selected as the insertion site. During the insertion of ARGs, disruption of *htrA* was utilized to enhance the tumor-targeting specificity and safety of VNP20009. To facilitate the efficient insertion of ARGs into the VNP20009 genome, we initially employed the CRISPR-Cas9 system for the primary insertion, followed by local optimization using the RED homologous recombination system.

For gas vesicles expression, ARGs composed of the auxiliary protein genes *gvpN-gvpU* from *Bacillus megaterium* and the structural protein genes *gvpA* and *gvpC* from the aquatic cyanobacterium *Anabaena flos-aquae* were selected (Fig. 1A). was observed using Transmission electron microscopy (TEM) revealed that the expression of ARGs in plasmids resulted in engineered bacteria filled with gas vesicles. Subsequently, ARGs transcribed under the *ptac* promoter were inserted into the VNP20009 genome, resulting in a strain named QARG-A1 (Fig. 1B). In QARG-A1, only a small number of gas vesicles were observed. Analysis of the transcription levels of *gvpA* and *gvpN* revealed that in QARG-A1, the transcription level of *gvpN* was only 1 %–2 % of that in the plasmid-expressed ARGs (Fig. 1C). To enhance the transcription level of the auxiliary protein gene, a separate *ptac* promoter was inserted before *gvpN*, leading to the construction of the strain named QARG-A2 (Fig. 1D). This modification increased the gas vesicles content within the bacteria and elevated the transcription level of *gvpN*, although plasmid-expressed ARGs still exhibited transcription levels 7 to 8 times higher than the genomic expression (Fig. 1E).

To further improve ARG transcription levels, the *ptac* promoter was replaced with the more active pT7 promoter. Using a plasmid system with galactose operon-regulated T7RNAP expression, we confirmed a positive correlation between T7RNAP expression levels and pT7-driven ARGs expression (Fig. S1). Since VNP20009 does not carry *T7RNAP*, *T7RNAP* was inserted into the VNP20009 genome. To maximize ARG transcription levels, we attempted to regulate T7RNAP using *ptac* but did not obtain positive clones, possibly due to adverse effects of sustained high-level T7RNAP expression on bacteria growth [35]. Therefore, we opted for dynamic regulation of T7RNAP using *plac* and CAP, inserting T7RNAP into the genome before ARGs, resulting in the strain named YQAP16 (Fig. 1F). CAP enhances *plac* transcription under glucose-free conditions, allowing YQAP16 to exhibit rigorous high or low gvp expression states, preventing stress from prolonged *gvp* expression. YQAP16 was cultured in LB medium without glucose, and TEM observations revealed that gas vesicles filled the cells uniformly. The transcription levels of *gvpA* and *gvpN* in YQAP16 had become similar to those expressed by plasmids (Fig. 1G). To validate CAP's regulatory capability over gas vesicles expression, YQAP16 was cultured in LB with varying glucose concentrations. In LB without glucose and with 0.1 % glucose, significant bacterial floating was oberved, but in LB with 1 % glucose, the number of floating bacteria sharply decreased, indicating reduced gas vesicles content (Fig. S2). This confirming CAP's effective control over gas vesicles expression in YQAP16. YQAP16 was propagated in LB with 1 % glucose to reduce strain growth burden, then cultured in LB with less than 0.1 % glucose for ultrasound imaging studies. Evaluations of gas vesicles expression stability in YQAP16 after continuous propagation and long-term storage followed by revival demonstrated stable gas vesicles expression (Fig. S3). Finally, we compared the growth rates of the constructed YQAP16 and VNP20009 at 37 °C. The results showed that the OD_{600} curves of YQAP16 and VNP20009 exhibited similar trends. However, considering that the gas vesicles expressed by YQAP16 increase the optical density of the bacteria, the growth rate of YQAP16 was 10 %–30 % lower than that of VNP20009, depending on the quantity of gas vesicles synthesized by YQAP16 (Fig. S4).

To evaluate YQAP16's ultrasound imaging capabilities, we used plasmid-expressed ARGs as a positive control and VNP20009 as a negative control for *in vitro* characterization. The ultrasound signals from YQAP16 were similar to those from plasmid-expressed ARGs (Fig. 1H). Ultrasound imaging at different YQAP16 concentrations revealed significant signals at 2.5×10^8 cfu/mL, increasing with concentration (Fig. S5). High-intensity focused ultrasound (HIFU) disrupted gas vesicles within the bacteria, causing ultrasound signal disappearance, confirming that signals originated from gas vesicles, detectable *in vivo* using this method (Fig. 1I). We further assessed YQAP16's *in vivo* ultrasound imaging effectiveness via intratumoral injection, with VNP20009 as a negative control. Before injection, no detectable signals were observed in either group. Post-injection, strong signals were only seen in the YQAP16 group, which were eliminated after HIFU treatment (Fig. 1J). This demonstrates that YQAP16 can be visualized *in vivo* through ultrasound imaging.

In conclusion, we successfully modified the tumor-targeting capabilities of the VNP20009 genome. The constructed YQAP16 exhibited ultrasound signals comparable to plasmid-expressed ARGs, confirming its detectability through *in vivo* ultrasound imaging.

2.2. In vivo effects of ultrasound-visualized engineered bacteria

To achieve the *in vivo* application of ultrasound-visualized engineered bacteria, we characterized and tested the safety dosage, tumor colonization efficiency, and targeting capability of YQAP16, followed by ultrasound imaging at the tumor site after tail vein injection of YQAP16. VNP20009 was used as a control to illustrate the modifications in the performance of YQAP16.

First, we assessed the safety dosage, starting with injection doses of 2.5×10^7 cfu and 5×10^7 cfu for the engineered bacteria. The dosage was adjusted based on the survival curves and weight changes of the mice (Fig. 2A). Mice injected with YQAP16 at doses ranging from 2.5×10^7 cfu to 1×10^8 cfu did not experience mortality, and their body weights increased over time. In contrast, mice injected with VNP20009 at a dose of 6.3×10^6 cfu exhibited mortality and continuous weight loss (Fig. 2B).

We also measured the residual concentration of the engineered bacteria in various organs, finding that at 24 h post-injection, the concentration of YQAP16 in each organ was approximately 10 % of that of VNP20009, indicating that YQAP16 is more readily cleared from the body. By day seven, the colonization levels of YQAP16 in the organs further decreased (Fig. 2C–S7).

To evaluate the inflammatory response in mice following injection of the engineered bacteria, we measured the concentrations of TNF-α and IL-6 in the blood. At the same dosage, the inflammation induced by YQAP16 was significantly lower than that caused by VNP20009. Notably, at an injection dose of 5×10^7 cfu, YQAP16 maintained a relatively low level of inflammation even on day seven. Therefore, the subsequent tail vein injection dosage for YQAP16 was set at 5×10^7 cfu (Fig. 2D–S7).

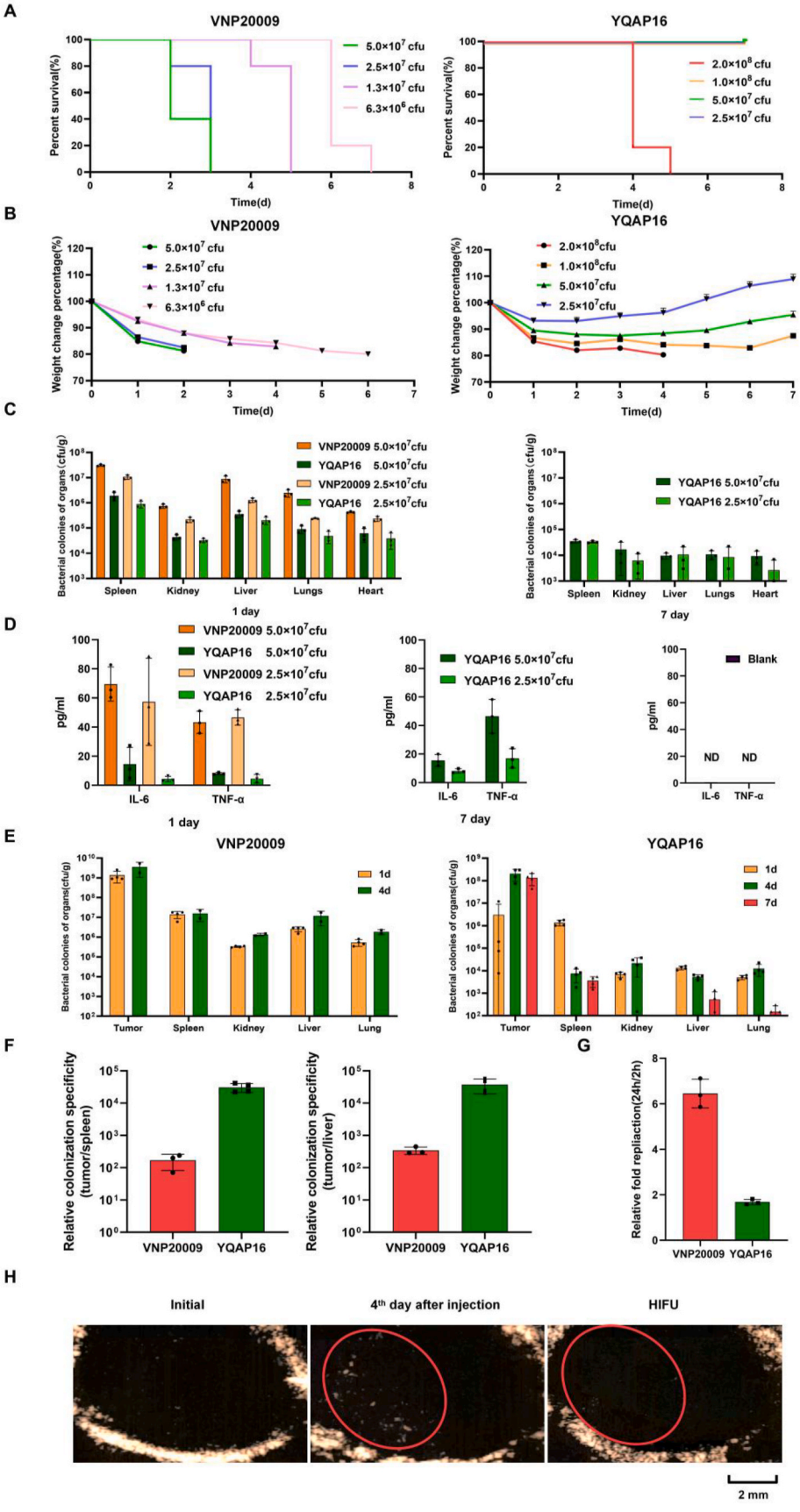

(caption on next page)

Fig. 2. Safety, tumor targeting, and *in situ* ultrasound imaging testing of ultrasound-visualized engineered bacteria in mice. (A) Survival curve of mice after injection of different doses of engineered bacteria. Death is marked when mouse weight decreases by more than 20 %. (n = 7). (B) Weight change curve of mice after injection of different doses of engineered bacteria. (n = 7, mice not included in statistics after death, data presented as mean ± SEM). (C) Bacterial colonization concentrations in various organs of mice after injection of different doses of engineered bacteria. (n = 3, data presented as mean ± SD). (D) Comparison of IL-6 and TNF-α levels in mouse plasma after injection of different doses of engineered bacteria, with "blank" representing healthy mouse plasma. (n = 3, data presented as mean ± SD). (E) Bacterial colonization concentrations in various organs of tumor-bearing mice after injection of engineered bacteria, with an injection dose of 5×10^7 cfu. (n = 4, two mice in the VNP20009 group died on the fourth day, only two were counted. Data presented as mean ± SD). (F) Analysis of the tumor targeting specificity of engineered bacteria. The ratio of bacterial concentration in the tumor to that in the spleen and liver is used to quantify the targeting specificity of engineered bacteria. (YQAP16, n = 4; VNP20009, n = 3. In the initial phase of the experiment, four mice were used as samples. During the experiment, two mice in the VNP20009 experimental group died, and one additional mouse sample was subsequently supplemented. Data presented as mean ± SD). (G) Replication rate of engineered bacteria in RAW267.4 macrophages. (n = 3, data presented as mean ± SD). (H) Ultrasound imaging of tumors after tail vein injection of engineered bacteria. "Initial" represents before injection of engineered bacteria, "4th day after injection" represents the fourth day after injection of engineered bacteria, and "HIFU" represents after HIFU explosion of gas vesicles on the fourth day after injection. The circled area indicates the region of ultrasound signal change. Scale bar, 2 mm.

We subsequently assessed the tumor colonization efficiency and targeting capability of YQAP16, using VNP20009 as a control. After the deletion of *htrA*, the tumor colonization efficiency of YQAP16 was significantly lower than that of VNP20009, with a colonization concentration at the tumor site on day one being below 1×10^7 cfu/g, which increased to 1×10^8 cfu/g in the following days. In contrast, VNP20009 achieved a concentration of 1×10^9 cfu/g on the first day (Fig. 2E). However, YQAP16 demonstrated a stronger clearance efficiency in non-tumor tissues. In non-tumor tissues, the spleen and liver showed higher colonization concentrations of the engineered bacteria. We measured the tumor-targeting specificity of the engineered bacteria by calculating the ratio of colonization concentration at the tumor site to that in the spleen or liver, finding that YQAP16 was approximately 100 times more specific than VNP20009 (Fig. 2F).

To confirm that *htrA* facilitates the growth of *Salmonella* within macrophages, we assessed the replication rates of YQAP16 and VNP20009 within macrophages. The replication rate of YQAP16 was approximately 30 % that of VNP20009, while both strains exhibited similar growth rates *in vitro* (Fig. 2G–S4). This characteristic may facilitate more efficient clearance of YQAP16 in normal tissues with immune cell infiltration, thereby reducing inflammation induced by engineered bacteria in normal tissues. On the other hand, due to the presence of an immune barrier in tumor tissues with only partial immune cell infiltration, YQAP16's colonization efficiency in tumor sites was minimally affected, ultimately leading to a significant enhancement in tumor-targeting specificity.

Finally, we tested the ultrasound imaging capabilities of YQAP16 at the tumor site following tail vein injection. On day four, a small amount of signal was observed during ultrasound imaging, which could be eliminated by HIFU (Fig. 2H). This indicates that YQAP16 can generate ultrasound signals in the tumor region via tail vein injection.

2.3. Development and performance characterization of ultrasound-based integrated diagnostic and therapeutic engineered bacteria

To achieve integrated engineering diagnostics and therapy, a plasmid expressing therapeutic proteins was introduced into YQAP16. To ensure the stable presence of the plasmid *in vivo*, the essential gene *thyA* was knocked out in YQAP16, and was complemented with the plasmid, resulting in the strain YQAP16T9 (Fig. 3A). After several passages, the plasmid remained stably maintained in YQAP16T9 (Fig. S8).

For tumor treatment studies, we selected therapeutic proteins, nbPD1 and nbCTLA-4. The plasmid was designed with a constitutive expression system using pRpL, and a secretion peptide, pelB, was added before the therapeutic gene to enhance protein secretion. A His tag was added to the C-terminus of nbPD1, and an HA tag was added to the C-terminus of nbCTLA-4 to facilitate protein expression detection. Western blot analysis of the supernatant from the centrifuged culture confirmed that nbPD1 and nbCTLA-4 were expressed and secreted into the culture medium (Fig. 3B).

Next, we confirmed the expression of *gvp* in YQAP16T9 carrying therapeutic components by assessing transcription levels of ARGs, TEM, and ultrasound imaging. Results indicated that YQAP16T9 maintained efficient expression of gas vesicles and generated ultrasound signals, with the transcription levels of ARGs comparable to those of the plasmid (Fig. 3C, D, 4E). Thus, the engineered ultrasonic visualized bacteria can effectively carry drug components for diagnosis and precise induction of bacterial treatment.

To test the efficacy of the engineered bacteria in tumor treatment, we injected them via the tail vein into mice. The mice show no significant weight loss (Fig. 3G), and tumor growth was inhibited with an inhibition rate of 50 %. This result indicates that the ultrasonic visualized engineered bacteria have a strong tumor-inhibitory effect when used alone. When the engineered bacteria carrying the drugs nbPD1 and nbCTLA-4, the tumor inhibition rate increased to about 65 % (Fig. 3H and I, S9), and the survival time was extended by more than double (Fig. 3J). Western blot analysis confirmed that the engineered bacteria could effectively express the drug proteins *in vivo* (Fig. 3K). This demonstrates that ultrasonic visualized engineered bacteria can carry drug components, further enhancing the therapeutic effect. In summary, the ultrasonic visualized engineered bacteria developed in this study can effectively target and treat tumors while carrying drug components for precise drug delivery.

3. Discussion

We have successfully developed an ultrasound-visible tumor-targeting engineered bacterium YQAP16 for theranostic research. This strain achieves stable genomic expression of ARGs, ensuring long-term expression stability while maintaining compatibility with therapeutic drug-carrying plasmids, providing a convenient platform for theranostic studies. Through expression system optimization, we have demonstrated that genomically expressed gas vesicles can achieve ultrasound imaging effects comparable to plasmid-based expression. In terms of safety, the deletion of the *htrA* gene has increased YQAP16's safety threshold by 10-fold and enhanced tumor-targeting specificity by 100-fold. This improvement significantly reduces off-target signal interference while substantially enhancing operational safety.

Animal experiments revealed certain limitations in the *in vivo* imaging performance of the constructed ultrasound-visible tumor-targeting bacteria. Specifically, ultrasound signals were prominent in intratumoral injections but showed insufficient contrast in tail vein injections. This phenomenon may be related to reduced colonization efficiency of the modified strain and the insufficient signal-to-noise ratio of the employed ARGs. To address this, we developed an innovative colonization strategy: transient *in vitro* induction of HtrA expression, enabling dynamic regulation that allows engineered bacteria to carry HtrA during initial injection, preventing rapid immune clearance and promoting rapid colonization; while non-colonizing bacteria are gradually cleared by the immune system during passage due to HtrA expression loss. This strategy enables efficient colonization of tumor sites by a large number of gas vesicle-rich engineered bacteria, achieving

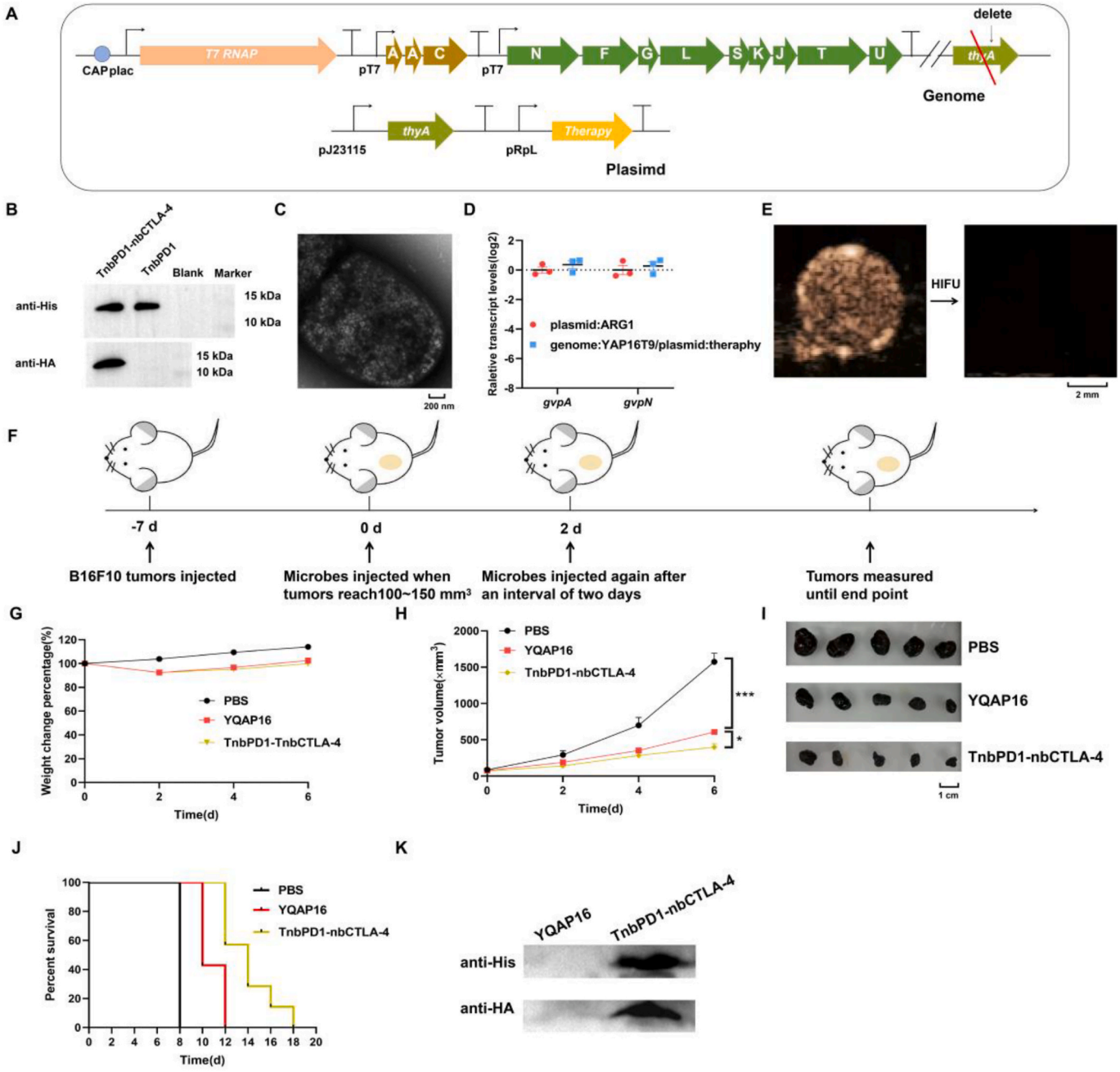

Fig. 3. Testing the effectiveness of drug-carrying ultrasound-visualized engineered bacteria in tumor treatment. (A) Schematic diagram of plasmid loss-induced lethal system construction. (B) Western blot analysis of drug protein secretion into the medium after culturing YQAP16T9 carrying drug plasmid in LB medium for 24 h. (C) TEM imaging of YQAP16T9 carrying drug plasmid. (D) Comparison of transcription levels of *gvpA* and *gvpN* between YQAP16T9 carrying drug plasmid and VNP20009 carrying ARGs plasmid. (n = 3, data presented as mean ± SEM). (E) Ultrasound imaging of YQAP16T9 carrying drug plasmid. The concentration of engineered bacteria is 1×10^9 cfu/mL. (F) Schematic diagram of the process of tumor treatment with engineered bacteria. (G) Weight change curve of mice after tail vein injection of engineered bacteria (n = 5, data presented as mean ± SEM). (H) Tumor volume change curve of mice (n = 5, data presented as mean ± SEM). (I) Images of tumors from each group. (J) Survival curve of mice (n = 7). (K) Western blot analysis of drug expression by engineered bacteria in tumors. Scale bars: 200 nm (C), 2 mm (E), 1 cm (J).

faster *in vivo* ultrasound localization (Fig. S10). Future studies could consider combining multiple strategies, such as quorum sensing regulation of HtrA and transient *in vitro* expression of capsular polysaccharides, to further enhance the delivery efficiency of engineered bacteria [28,36]. To address the insufficient signal-to-noise ratio of ARG1, it could be replaced with bARGser, which offers higher signal-to-noise ratio. Although the bARGser gene cluster is twice the size of ARG1, increasing the difficulty of genomic knock-in, its expression strategy can be adapted from our current approach, utilizing the pT7 promoter to drive ARGs transcription while regulating T7RNAP expression levels to control transcriptional intensity.

In recent years, with the advancement of precision drug delivery research, scientists have developed ultrasound biological components and focused ultrasound remote-controlled drug release systems, enabling targeted drug release based on engineered bacteria localization. However, current systems with both ultrasound and drug components located on plasmids are affected by the dual-plasmid system's impact on *in vivo* drug and ultrasound signal output [37]. The

ultrasound-visible tumor-targeting engineered bacteria developed in this study effectively addresses this issue, achieving excellent compatibility between the two components. We believe that with continuous optimization, ultrasound-visible tumor-targeting engineered bacteria will become important therapeutic vectors, providing robust support for real-time *in vivo* monitoring and precise theranostic applications.

4. Materials and methods

4.1. Cell lines and animal models

The B16–F10 tumor cells (Catalog No. TCM36) and RAW264.7 cells (Catalog No. TCM13) were obtained from National Collection of Authenticated Cell Cultures. B16–F10 tumor cells and RAW264.7 cells were cultured DMEM medium (meilunbio, Catalog No. MA0212) with 10 % FBS (meilunbio, Catalog No. PWL001) and 1 % penicillin/streptomycin. The cells were incubated at 37 °C with 5 % CO_2.

Female C57BL/6J mice in 6∼8 weeks were purchased from Shanghai Model Organisms Center, Inc. All animal experiment procedures were approved by East China University of Science and Technology, and were performed in strict accordance with the Guidelines for Care and Use of Laboratory Animals [ECUST-21038]. The experiments and all efforts were made to minimize suffering.

4.2. Plasmid construction

This study involves three types of plasmids: the acoustic report plasmid expressing ARGs, the editing plasmid for genome knock-in, and the drug-expressing plasmid. All three plasmids were constructed in DH5α through Gibson assembly and then tested in Salmonella. In the construction of the acoustic report plasmid for ARGs, we cloned the *gvpA* and *gvpC* genes from *A. flosaquae* and the *gvpNFGLSKJTU* gene cluster from *B. megaterium* into the backbone of pTD103-ARG1. Compared to ARG1, we removed the ineffective *gvpR* gene from the front end of *B. megaterium*. In the genome knock-in editing plasmid, we selected the CRISPR-Cas9 editing system, with the sgRNA recognition site chosen in *htrA*, and the insertion sequence being ARGs regulated by ptac. Two 1000 bp homologous arms were designed, and the sgRNA recognition site and homologous arm sequences are shown in Table S2. For the drug-expressing plasmid, we used the pMA-thermal_CTLA-4 plasmid backbone, with the promoter pRpL regulating the expression of nbPD1 and nbCTLA-4 (Table S1).

4.3. Gene knock-in

This study involves two genome editing methods. First, the ARGs were knocked into the genome using the CRISPR-Cas9 genome editing plasmid, and the CRISPR-Cas9 editing plasmid was removed through continuous passage (Table S2). Then, using the plasmid pKD46 with the RED recombination system, the expression of ARGs in the genome was optimized by connecting 50 bp∼100 bp homologous arms before and after the knock-in fragments. After gene knock-in, the RED recombination system plasmid was lost through continuous passage at 42 °C.

4.4. Bacterial expression

The culture medium used for the engineered bacteria to express gas vesicles is LB. Initially, the strain is activated in 5 mL of LB at 37 °C for 12 h, followed by transferring 1 % to new medium. It is then cultured at 37 °C until the OD_{600} reaches 0.4–0.6, and subsequently placed at 30 °C for 24 h. VNP20009 carrying pTD103-ARG is induced with 30 nM AHL, while ARG-A1, ARG-A2, YQAP16, and YQAP16T9 carrying drug plasmids do not require an inducer. Additionally, YQAP16 and YQAP16T9 carrying drug plasmids use 1 % Glc in routine passage.

4.5. TEM sample preparation and imaging

The engineered bacteria expressing gas vesicles are centrifuged at low speed (600×*g*) to collect the floating bacteria. If no floating bacteria are present, the sedimented bacteria are collected. The bacteria are resuspended in deionized water, repeated once to remove the medium, and then the solution is dropped onto a carbon grid. The samples are stained with phosphotungstic acid and imaged using TEM JEM-2100.

4.6. Bacterial density conversion

The sedimented and floating bacteria are collected, adjusted to an OD_{600} of 0.5, diluted, and plated for counting. The density of bacteria expressing different states of gas vesicles is recorded. As the expression of gas vesicles increases, the bacterial density at the same OD_{600} is lower, with floating YQAP16 being about 25 % of VNP20009 that completely does not express gas vesicles (Fig. S4). Therefore, when calculating the injection dose or bacterial density, the state of gas vesicle expression must be considered. The engineered bacteria are first adjusted to an $OD_{600} = 0.5$, and then diluted or concentrated based on the plate count data.

4.7. In vitro ultrasound imaging

Dissolve 1 % (W/V) agarose in PBS, pour it into a mold with inserted EP tubes, and let it cool. Once the 1 % (W/V) agarose has solidified, remove the EP tubes and cut the agarose for later use. Inject the collected engineered bacteria into the cavity formed by the EP tubes, and perform bacterial ultrasound contrast imaging using VisualSonics Vevo 2100 (VisualSonics, Inc., USA). The ultrasound parameters are 18 MHz and 90 % power.

4.8. Mouse tumor inoculation

Select 6∼8-week-old female C57BL/6J mice, allow them to acclimate for one week, and then inoculate them with 1×10^6 B16F10 cells. When the tumor volume reaches 50–150 mm^3, prepare to inject the engineered bacteria. Euthanize the mice when the tumor volume exceeds 2000 mm^3. Tumor volume is approximated using the formula $a \times b^2/2$, where a represents the longest dimension of the tumor and b represents the shortest dimension.

4.9. Engineered bacteria tissue colonization calculation

Weigh the collected tissue post-dissection, add 200 μL of PBS for every 0.1 g of tissue, and homogenize the tissue using a tissue homogenizer. Plate dilutions are made after homogenization, assuming that the volume of the homogenate is approximately 300 μL, and calculate the colonization density of the engineered bacteria.

4.10. Measurement of IL-6 and TNF-α in blood

Collect mouse blood into EP tubes by enucleating the eyes and let it sit at room temperature for 30 min. Centrifuge the blood at 3000 rpm for 20 min and collect the upper serum. Determination of IL-6 and TNFα levels by ELISA.

4.11. Testing the replication rate of bacteria within macrophages

Collect RAW267.4 cells and plate them in a 24-well plate. When the cells cover 70 % of the area, add the bacterial suspension at a multiplicity of infection (MOI) of 10:1. In this experiment, each well contains approximately 1×10^6 cells, and 1×10^7 cfu of bacteria are added. Incubate the RAW267.4 cells in DMEM medium containing bacteria for 30 min, discard the medium, and wash with PBS. Add DMEM medium containing 50 μg/mL gentamicin to kill bacteria that have not been

phagocytosed by macrophages. After 2 and 24 h of incubation, discard the medium, wash with PBS, collect the cells, lyse them with 1 % Triton X-100, and plate dilutions to calculate the bacterial load. The replication rate of bacteria within macrophages is calculated by dividing the number of bacteria in RAW267.4 cells after 24 h by the number after 2 h (24 h/2 h).

4.12. *In vivo* ultrasound imaging

This study involves two methods for establishing bacterial colonization in tumors for ultrasound imaging: intratumoral injection and tail vein injection. The injection dose of engineered bacteria is 100 μL of a 5×10^8 cfu suspension. Intratumoral injection allows for immediate ultrasound imaging, while tail vein injection permits ultrasound imaging on the fourth day post-injection. The ultrasound imaging parameters and modes are the same as for *in vitro* imaging.

4.13. *Drug protein secretion detection*

Detect the secretion of nbPD1 and nbCTLA-4 using Western blot. For *in vitro* analysis, collect the culture medium of engineered bacteria carrying drug plasmids after 24 h of expression at 37 °C. For *in vivo* analysis, collect tumor tissues, add 100 μL of cell lysis buffer per 0.1 g of tissue, homogenize the tissues, and centrifuge to collect the supernatant for analysis.

CRediT authorship contribution statement

Li Qu: Writing – review & editing, Writing – original draft, Validation, Methodology, Investigation, Conceptualization. **Zhou Chi:** Validation. **Zhen-Ping Zou:** Writing – review & editing. **Ying Zhou:** Writing – review & editing. **Bang-Ce Ye:** Writing – review & editing, Conceptualization.

Declaration of competing interest

The authors declare that they have no competing interests.

Acknowledgments

This work was sponsored by the National Key Research and Development Program of China (2020YFA0908800) and the National Natural Science Foundation of China (22134003). Special thanks to Professor Yan Fei from the Shenzhen Institute of Advanced Technology for providing the ultrasound imaging equipment.

Appendix A. Supplementary data

Supplementary data to this article can be found online at https://doi.org/10.1016/j.synbio.2025.03.009.

References

[1] Steidler L, Hans W, Schotte L, Neirynck S, Obermeier F, Falk W, et al. Treatment of murine colitis by *Lactococcus lactis* secreting interleukin-10. Science 2000;289(5483):1352–5. https://doi.org/10.1126/science.289.5483.1352.
[2] Claesen J, Fischbach MA. Synthetic microbes as drug delivery systems. ACS Synth Biol 2015;4(4):358–64. https://doi.org/10.1021/sb500258b.
[3] Din MO, Danino T, Prindle A, Skalak M, Selimkhanov J, Allen K, et al. Synchronized cycles of bacterial lysis for *in vivo* delivery. Nature 2016;536(7614):81–5. https://doi.org/10.1038/nature18930.
[4] Forbes NS, Munn LL, Fukumura D, Jain RK. Sparse initial entrapment of systemically injected *Salmonella typhimurium* leads to heterogeneous accumulation within tumors. Cancer Res 2003;63(17):5188–93. https://doi.org/10.1097/00130404-200309000-00013.
[5] Kasinskas RW, Forbes NS. *Salmonella typhimurium* specifically chemotax and proliferate in heterogeneous tumor tissue *in vitro*. Biotechnol Bioeng 2006;94(4):710–21. https://doi.org/10.1002/bit.20883.
[6] Zhao M, Yang M, Li X-M, Jiang P, Baranov E, Li S, et al. Tumor-targeting bacterial therapy with amino acid auxotrophs of GFP-expressing *Salmonella typhimurium*. Proc Natl Acad Sci USA 2005;102(3):755–60. https://doi.org/10.1073/pnas.0408422102.
[7] Streilein JW. Unraveling immune privilege. Science 1995;270(5239):1158–9. https://doi.org/10.1126/science.270.5239.1158.
[8] Westphal K, Leschner S, Jablonska J, Loessner H, Weiss S. Containment of tumor-colonizing bacteria by host neutrophils. Cancer Res 2008;68(8):2952–60. https://doi.org/10.1158/0008-5472.CAN-07-2984.
[9] Cooper RM, Wright JA, Ng JQ, Goyne JM, Suzuki N, Lee YK, et al. Engineered bacteria detect tumor DNA. Science 2023;381(6658):682–6. https://doi.org/10.1126/science.adf3974.
[10] Chen Y, Li ZH, Zeng X, Zhang XZ. Bacteria-based bioactive materials for cancer imaging and therapy. Adv Drug Deliv Rev 2023;193. https://doi.org/10.1016/j.addr.2023.114696.
[11] Danino T, Prindle A, Kwong GA, Skalak M, Li H, Allen K, et al. Programmable probiotics for detection of cancer in urine. Sci Transl Med 2015;7(289). https://doi.org/10.1126/scitranslmed.aaa3519. 289ra84-ra84.
[12] Gurbatri CR, Radford GA, Vrbanac L, Im J, Thomas EM, Coker C, et al. Engineering tumor-colonizing *E. coli* Nissle 1917 for detection and treatment of colorectal neoplasia. Nat Commun 2024;15(1):646. https://doi.org/10.1038/s41467-024-44776-4.
[13] Donaldson GP, Lee SM, Mazmanian SK. Gut biogeography of the bacterial microbiota. Nat Rev Microbiol 2016;14(1):20–32. https://doi.org/10.1038/nrmicro3552.
[14] Yoo SW, Nguyen DH, Park S, Lee H, Lee CM, Lee C, et al. Development of dual-scale fluorescence endoscopy for *in vivo* bacteria imaging in an orthotopic mouse colon tumor model. Appl Sci 2020;10(3):844. https://doi.org/10.3390/app10030844.
[15] Min JJ, Nguyen VH, Kim HJ, Hong YJ, Choy HE. Quantitative bioluminescence imaging of tumor-targeting bacteria in living animals. Nat Protoc 2008;3(4):629–36. https://doi.org/10.1038/nprot.2008.32.
[16] Yun M, You SH, Nguyen VH, Prakash J, Glasl S, Gujrati V, et al. Reporter gene-based optoacoustic imaging of targeted colon cancer *in vivo*. Sci Rep 2021;11(1):24430. https://doi.org/10.1038/s41598-021-04047-4.
[17] Bourdeau RW, Lee-Gosselin A, Lakshmanan A, Farhadi A, Kumar SR, Nety SP, et al. Acoustic reporter genes for noninvasive imaging of microorganisms in mammalian hosts. Nature 2018;553(7686):86–90. https://doi.org/10.1038/nature25021.
[18] Foucault M-L, Thomas L, Goussard S, Branchini B, Grillot-Courvalin C. *In vivo* bioluminescence imaging for the study of intestinal colonization by *Escherichia coli* in mice. Appl Environ Microbiol 2010;76(1):264–74. https://doi.org/10.1128/AEM.01686-09.
[19] Daniel C, Poiret S, Dennin V, Boutillier D, Pot B. Bioluminescence imaging study of spatial and temporal persistence of *Lactobacillus plantarum* and *Lactococcus lactis* in living mice. Appl Environ Microbiol 2013;79(4):1086–94. https://doi.org/10.1128/AEM.03221-12.
[20] Chu J, Oh Y, Sens A, Ataie N, Dana H, Macklin JJ, et al. A bright cyan-excitable orange fluorescent protein facilitates dual-emission microscopy and enhances bioluminescence imaging *in vivo*. Nat Biotechnol 2016;34(7):760–7. https://doi.org/10.1038/nbt.3550.
[21] Smith-Bindman R, Miglioretti DL, Johnson E, Lee C, Feigelson HS, Flynn M, et al. Use of diagnostic imaging studies and associated radiation exposure for patients enrolled in large integrated health care systems, 1996-2010. JAMA 2012;307(22):2400–9. https://doi.org/10.1001/jama.2012.5960.
[22] Errico C, Pierre J, Pezet S, Desailly Y, Lenkei Z, Couture O, et al. Ultrafast ultrasound localization microscopy for deep super-resolution vascular imaging. Nature 2015;527(7579):499–502. https://doi.org/10.1038/nature16066.
[23] Farhadi A, Ho GH, Sawyer DP, Bourdeau RW, Shapiro MG. Ultrasound imaging of gene expression in mammalian cells. Science 2019;365(6460):1469–75. https://doi.org/10.1126/science.aax4804.
[24] Hurt RC, Buss MT, Duan M, Wong K, You MY, Sawyer DP, et al. Genomically mined acoustic reporter genes for real-time *in vivo* monitoring of tumors and tumor-homing bacteria. Nat Biotechnol 2023;41(7):919–31. https://doi.org/10.1038/s41587-022-01581-y.
[25] Pfeifer F. Distribution, formation and regulation of gas vesicles. Nat Rev Microbiol 2012;10(10):705–15. https://doi.org/10.1038/nrmicro2834.
[26] Dutka P, Metskas LA, Hurt RC, Salahshoor H, Wang T-Y, Malounda D, et al. Structure of *Anabaena flos-aquae* gas vesicles revealed by cryo-ET. Structure 2023;31(5):518–28. https://doi.org/10.1016/j.str.2023.03.011.
[27] Zhang X, Xu Q, Yang L, Lai Y, Zhang Z, Han C, et al. The genes *slyA, STM3120* and *htrA* are required for the anticancer ability of VNP20009. Oncotarget 2016;7(49):81187. https://doi.org/10.18632/oncotarget.13217.
[28] Wu L, Li L, Qiao L, Li C, Zhang S, Yin X, et al. Programmable bacteria with dynamic virulence modulation system for precision antitumor immunity. Adv Sci 2024;11(36):2404069. https://doi.org/10.1002/advs.202404069.
[29] Jinek M, Chylinski K, Fonfara I, Hauer M, Doudna JA, Charpentier E. A programmable dual-RNA-guided DNA endonuclease in adaptive bacterial immunity. Science 2012;337(6096):816–21. https://doi.org/10.1126/science.1225829.
[30] Cong L, Ran FA, Cox D, Lin S, Barretto R, Habib N, et al. Multiplex genome engineering using CRISPR/Cas systems. Science 2013;339(6121):819–23. https://doi.org/10.1126/science.1231143.
[31] Zhang Y, Buchholz F, Muyrers JP, Stewart AF. A new logic for DNA engineering using recombination in *Escherichia coli*. Nat Genet 1998;20(2):123–8. https://doi.org/10.1038/2417.
[32] Busby S, Ebright RH. Transcription activation by catabolite activator protein (CAP). J Mol Biol 1999;293(2):199–213. https://doi.org/10.1006/jmbi.1999.3161.

[33] Wu L, Li L, Li S, Liu L, Xin W, Li C, et al. Macrophage-mediated tumor-targeted delivery of engineered *Salmonella typhimurium* VNP20009 in anti-PD1 therapy against melanoma. Acta Pharm Sin B 2022;12(10):3952–71. https://doi.org/10.1016/j.apsb.2022.05.006.

[34] Abedi MH, Yao MS, Mittelstein DR, Bar-Zion A, Swift MB, Lee-Gosselin A, et al. Ultrasound-controllable engineered bacteria for cancer immunotherapy. Nat Commun 2022;13(1):1585. https://doi.org/10.1038/s41467-022-29065-2.

[35] Du F, Liu YQ, Xu YS, Li ZJ, Wang YZ, Zhang ZX, et al. Regulating the T7 RNA polymerase expression in BL21 (DE3) to provide more host options for recombinant protein production. Microb Cell Fact 2021;20(1):1–10. https://doi.org/10.1186/s12934-021-01680-6.

[36] Harimoto T, Hahn J, Chen Y-Y, Im J, Zhang J, Hou N, et al. A programmable encapsulation system improves delivery of therapeutic bacteria in mice. Nat Biotechnol 2022;40(8):1259–69. https://doi.org/10.1038/s41587-022-01244-y.

[37] Yang Y, Wang Y, Zeng F, Chen Y, Chen Z, Yan F. Ultrasound-visible engineered bacteria for tumor chemo-immunotherapy. Cell Rep Med 2024:101512. https://doi.org/10.1016/j.xcrm.2024.101512.